

Supplementary Materials for

Core/Shell Nanocomposites Produced by Superfast Sequential Microfluidic Nanoprecipitation

Dongfei Liu^{*,†,‡}, Hongbo Zhang^{†,‡}, Salvatore Cito[†], Jin Fan[§], Ermei Mäkilä[¶], Jarno Salonen[¶],
Jouni Hirvonen[†], Tiina M. Sikanen[†], David A. Weitz[‡] and Hélder A. Santos^{*,†}

[†]Division of Pharmaceutical Chemistry and Technology, Faculty of Pharmacy, University of Helsinki, FI-00014 Helsinki, Finland.

[‡]John A. Paulson School of Engineering and Applied Sciences, Harvard University, 02138, Cambridge, MA, USA.

[§]Department of Orthopaedics, The First Affiliated Hospital of Nanjing Medical University, 210029 Nanjing, China.

[¶]Laboratory of Industrial Physics, Department of Physics and Astronomy, University of Turku, FI-20014 Turku, Finland.

*Correspondence to: dongfei.liu@helsinki.fi (D. L.) and helder.santos@helsinki.fi (H. A. S.).

MATERIALS AND METHODS

Fabrication of the microcapillary device. The microfluidic co-flow capillary device was fabricated by assembling three coaxial aligned borosilicate glass capillaries (World Precision Instruments, Inc.) on a glass slide (Figure 1A). One end of the cylindrical capillaries 1 (C1; inner diameter, i.d., ~580 μm and outer diameter, o.d., ~1000 μm) and 2 (C2; i.d. 1100 μm and o.d. 1500 μm) was tapered using a micropipette puller (P-97, Sutter Instrument Co., USA) to a diameter of 20 μm ; this diameter was further enlarged to ~90 μm . The tapered C1 was inserted into the tapered C2. These two tapered glass capillaries were then inserted into the biggest cylindrical capillary 3 (C3; i.d. 1600 μm). A transparent epoxy resin (5 min Epoxi, Devcon) was used to seal the capillaries where required. In this co-flow geometry, all three fluids flow in the same direction. The inner fluid 1 (F1; drug and polymer solution) flows in the space between the two tapered cylindrical capillaries C1 and C2, while the aqueous fluids F2 and F3 flow inside C2 and C3, respectively.

Reynolds number (Re) and flow imaging. The flow rates through the microfluidic device were regulated by mounting three syringes on syringe pumps. Re was calculated using the following eq S1:

$$Re = \frac{\rho UL_0}{\mu} = \frac{\rho Q}{\mu E} \quad (\text{S1})^1$$

where, μ is the viscosity of fluid, ρ represents the density of the fluid, U is the velocity of the fluid, Q represents the flow rate, and E is the channel diameter of the capillary.

Flow patterns in the microfluidic device were imaged using a light microscope (EVOS[®] 1 \times , Thermo Fisher Scientific Inc., USA) as a function of Re (varied from 10 to 1300) and flow ratios. The ratios, 1:2:6 and 1:5:30, represent the flow ratio among inner fluids 1 (F1) and 2 (F2) and

outer fluid 3 (F3). To facilitate the visualization of the flow patterns in the mixing zone, the bromophenol blue was added into F1.

Computational fluid dynamics (CFD) simulation. As previously explained, our experimental setup is able to qualitatively visualize the flow pattern in the mixing zone. However, it is challenge to quantitatively measure the residence time of dyes in the timescale of several milliseconds. To overcome this technological pitfall, the flow patterns of this microfluidic nanoprecipitation platform were simulated and predicted using CFD. The mass transfer rates of this platform were all calculated in terms of Re and flow ratios. To perform this CFD simulation, we used the finite element commercial code “COMSOL” to numerically solve the steady momentum (eqs S2 and S3):

$$\rho(\vec{u}\nabla)\vec{u} = \nabla \cdot \left[-pI + \mu \left(\nabla\vec{u} + (\nabla\vec{u})^T - \frac{2}{3}\mu(\nabla \cdot \vec{u})I \right) \right] \quad (\text{S2})$$

$$\nabla \cdot (\rho\vec{u}) = 0 \quad (\text{S3})$$

and the mass transfer in eq S4, which includes the diffusion and convection of a diluted specie:

$$\frac{dc}{dt} + \nabla \cdot (-D\nabla c) + u \cdot \nabla c = 0 \quad (\text{S4})$$

where \vec{u} is the velocity vector, p represents the pressure, D is the diffusivity of the diluted specie and c is the concentration of the diluted specie. The differential equation of our model is solved imposing normal inflow velocity and a constant reactant concentration at inlets, and constant pressure and zero diffusion flux of the reactant at the outlet and non-slip condition at the walls.

With Re higher than 100, CFD model does not converge due to the presence of time dependent instability that might need to be solved using Direct Navier Stokes (DNS method). However, DNS is computationally too demanding. To overcome this, the K-epsilon turbulence model was employed to numerically solve the turbulent jet (eqs S5–S10). The turbulent viscosity is modeled as following:

$$\rho(\vec{u}\nabla)\vec{u} = \nabla \cdot [-pI + (\mu + \mu_T)(\nabla\vec{u} + (\nabla\vec{u})^T)] + F \quad (\text{S5})$$

$$\rho\nabla \cdot (\vec{u}) = 0 \quad (\text{S6})$$

$$\rho(\vec{u}\nabla)k = \nabla \cdot \left[\left(\mu + \frac{\mu_T}{\sigma_k} \right) \nabla k \right] + P_k - \rho\epsilon \quad (\text{S7})$$

$$\rho(\vec{u}\nabla)\epsilon = \nabla \cdot \left[\left(\mu + \frac{\mu_T}{\sigma_\epsilon} \right) \nabla \epsilon \right] + C_\epsilon \frac{\epsilon}{k} P_k - C_{\epsilon 2} \rho \frac{\epsilon^2}{k}, \epsilon = ep \quad (\text{S8})$$

$$\mu_T = \rho C_\mu \frac{K^2}{\epsilon} \quad (\text{S9})$$

$$P_k = \mu_T [\nabla\vec{u} : (\nabla\vec{u} + (\nabla\vec{u})^T)] \quad (\text{S10})$$

where C_μ is a model constant, k is the turbulent kinetic energy, ϵ is the turbulent dissipation rate, ep represents the turbulent dissipation rate, σ_k and σ_ϵ are turbulent Prandtl number for k and ϵ , C_μ and C_ϵ are constants in the turbulence transport eq S8, μ_T represents the dynamic eddy viscosity and P_k is the production of k .

Residence time distribution (RTD). The RTD of the drug nanocrystals in C1 was computed as the probability distribution function, which defines the amount of time that the particle can spend inside the C1. RTD is used here to characterize the time different between the first and second precipitation process under different inflow conditions.

The RTD is represented by an exit age distribution, $E(t)$. The function $E(t)$ has the units of time^{-1} and is defined as in eq S11:

$$E(t) = \frac{N(t)}{\int_0^{\infty} N(t)dt} \quad (\text{S11})$$

where, $N(t)$ is the average number of drug nanocrystals inside C1. Note that the function $E(t)$ has the following property in eq S12:

$$\int_0^{\infty} E(t)dt = 1 \quad (\text{S12})$$

Additionally, the first and the second central moments of the age distribution function $E(t)$ are respectively the average residence time τ_m and the variance (σ^2) which gives an indication on the degree of dispersion around the mean, as shown in eqs S13–S14:

$$\tau_m = \int_0^{\infty} tE(t)dt \quad (\text{S13})$$

$$\sigma^2 = \int_0^{\infty} (t - \tau_m)^2 E(t)dt \quad (\text{S14})$$

Solubility diagrams. To aid the successful development of core/shell nanocomposites, we studied the solubility profiles of paclitaxel (PTX; >98%, Suzhou Famu Pharmaceutical Technology Co., Ltd, China), sorafenib (SFN; >99%, LC Laboratories, USA) and HF in a series mixtures of solvent (acetone) and non-solvent (water). The solubility diagrams were therefore constructed to guide the selection of flow ratios among all three fluids to enable the sequential nanoprecipitation of nanocomposite precursor. Specifically, a series of water was added into the acetone solution

containing PTX or SFN with an initial concentration of 10 mg/mL. In the next step, the freshly formed drug nanocrystals were removed by centrifugation (16500g, 5 min). The amounts of dissolved PTX and SFN in supernatants were quantified by high performance liquid chromatography (HPLC) using an Agilent 1100 (Agilent Technologies, USA) with a mobile phase composed of water and acetonitrile (35:65, v/v). The flow rate of the mobile phase was 1.0 mL/min and the temperature was set at 30 °C, using a Kinetex[®] EVO C₁₈ column (4.6×150 mm, 5 μm; Phenomenex Inc., USA) as the stationary phase. The detection wavelength of 227 nm was selected for PTX and 265 nm for SFN, and the sample injection volume was 20 μL.

To enable its quantitative analysis, Alexa Fluor[®] 488 hydrazide (AF488)-labelled HF (AF488-HF) was synthesized based on 1-ethyl-3-(3-dimethylaminopropyl)-carbodiimide/N-hydroxysuccinimide (EDC/NHS, Thermo Fisher Scientific, USA) conjugation chemistry. First, HF in dimethylformamide solution (20 mg/mL) was activated by adding excess EDC and NHS for 24 h. Next, the excess amount of AF488 hydrazide was reacted with the activated HF for 24 h. In the following step, water was added to precipitate the AF488-labelled HF. After centrifugation (16000g, 10 min), the resulting pellet was washed twice thoroughly with water by vortexing and sonication followed by centrifugation and removal of supernatants. Residual water was removed by lyophilization and the AF488-labelled HF was finally obtained. A series of water (pH 3 or 10.4) was added into the AF488-HF acetone solution (10 mg/mL). The precipitated HF particles were removed by centrifugation (16500g, 5 min). The fluorescence intensity of dissolved AF488-labelled HF in supernatant was measured on a Varioskan Flash fluorometer (Thermo Fisher Scientific, USA). All the experiments were performed at least in triplicate.

Preparation of drug nanocrystals and core/shell nanocomposites. The single microfluidic nanoprecipitation approach has been employed to prepare the bare drug nanocrystals at room temperature, as described elsewhere². In general, a PTX or SFN drug acetone solution (10 mg/mL) and an aqueous solution served as the outer and inner fluids, respectively. The inner (4.21 mL/min) and outer fluids (0.42 mL/min) were separately pumped into the microfluidic device, flowing in the same direction. Drug molecules assembled into particles during diffusion from acetone to water, and thus, the drug nanocrystals formed.

We prepared the core/shell nanocomposites through a superfast sequential microfluidic nanoprecipitation platform. A drug acetone solution (10 mg/mL) containing HF (10 mg/mL) was used as the inner fluid 1 (F1), a basic aqueous solution (pH 10.4) served as the inner fluid 2 (F2), and an acidic aqueous solution (pH 3) served as the outer fluid (F3). First, the inner F1 was mixed with F2 to form the drug nanocrystals. This drug nanoparticle suspension containing dissolved HF was immediately mixed with F3. Due to the decrease of pH values, the dissolved HF precipitated and deposited onto the surface of freshly formed drug nanocrystals. Finally, the drug nanocrystal encapsulated core/shell nanocomposite with a ratio of 1:1 formed. The effect of Re (varied from 10 to 1300) on the particle size and size distribution of obtained nanocomposites was also studied. During the nanomaterials synthesis, the flow rates were controlled by syringe pumps. The resulting nanomaterial suspension was washed triple with water by ultrafiltration (6000g, 15 min) with a membrane of nominal molecular weight limit of 100 kDa (Amicon[®] Ultra; Merck Millipore Ltd.) to remove the organic solvents and unencapsulated drugs.

Regarding the preparation of the nanocomposite with a PLGA core, PLGA acetonitrile solution containing HF, acetalated dextran (AcDX),³ or spermine-modified acetalated dextran (AcDXSP)⁴ served as F1. To avoid the precipitation of shell polymers at the first mixing process, ethanol

solution containing water (20%, v/v) was used as F2. The PLGA cores formed at first by mixing F1 with F2. Due to their high solubility in ethanol, no precipitation of AcDX, AcDXSP or HF occurred at this stage. This PLGA ethanol suspension containing dissolved AcDX, AcDXSP or HF was then mix with another aqueous solution, in which the AcDX, AcDXSP or HF precipitated and deposited onto the surface of freshly formed PLGA cores. In terms of the preparation of AcDXSP@HF, AcDXSP and HF ethanol solution served as F1 and the rest procedures were the same with the synthesis of PTX@HF nanocomposites.

Characterization of fabricated nanomaterials. The structure of the fabricated nanocomposites was evaluated by transmission electron microscope (TEM; Tecnai 12, FEI Company, USA) at an acceleration voltage of 120 kV. The TEM samples were prepared by depositing 2 μ L of the nanoparticle suspensions (1.0 mg/mL) onto carbon-coated copper grids (300 mesh; Electron Microscopy Sciences, USA). Samples were blotted away after 5 min incubation, and the grids were then washed twice with distilled water and air-dried prior to imaging.

The surface morphology of the nanocomposites was studied using scanning electron microscopy (SEM; Ultra-55, Zeiss EVO) at room temperature at an accelerating voltage of 5 kV. All the samples were platinum coated in a high vacuum evaporator (Q150TS, Quorum Technologies, UK) before imaging. The particle size of obtained nanocomposites was analyzed by the dynamic light scattering method (Zetasizer Nano ZS, Malvern Instruments Ltd., UK) at an angle of 173° and at 25 °C.

The size evolution of bare drug nanocrystals and core/shell nanocomposites in term of time has been studied for 30 days (1 month) at 4 °C. The average size of freshly prepared nanomaterials

served as the control. The particle size was determined by the dynamic light scattering method and the surface morphology was studied by SEM.

Differential scanning calorimeter (DSC) was used to study the state of the loaded therapeutics in PTX@HF and SFN@HF after lyophilization. The DSC analysis was performed with a Pyris Diamond DSC (PerkinElmer, USA) using a heating rate of 10.0 °C/min under N₂ gas purge of 40 mL/min, in aluminum sample pans with pierced covers. The X-ray diffraction (XRD) measurements were performed with a X'Pert PRO (PANalytical, Netherlands) diffractometer in Bragg-Brentano geometry using a PIXcel^{1D} detector in scanning line mode with Cu(K α) radiation. The interaction between payloads and HF was characterized by Fourier transform infrared (FTIR, Vertex 70, Bruker, USA), using a horizontal attenuated total reflectance (ATR) accessory (MIRacle, PIKE Technologies, USA). The FTIR spectra were recorded at room temperature between 4000-650 cm⁻¹ with a resolution of 4 cm⁻¹ using OPUS 5.5 software.

Drug loading degrees and in vitro drug release tests. The loading degrees for the obtained nanomaterials were determined by immersing them into acetonitrile to dissolve the polymeric matrix and release all the payloads. The amount of PTX and SFN was quantified by HPLC, as described above. The *in vitro* release of PTX and SFN from different formulations was evaluated in buffer solutions with pH values of 1.2, 5.0 and 7.4, respectively. A solution with a two-step change of pH values from 1.2 to 7.4 has also been utilized to evaluate the release of payloads from the prepared nanomaterials. Owing to their low aqueous solubility, fetal bovine serum (FBS; 10%, v/v) was added into the release medium to solubilize PTX and SFN. The nanomaterials (~100 μ g) was put into buffer solution (50 mL) using a shaking method at 100 rpm and 37 \pm 1 °C. Because of their poor colloid stability, freshly prepared bare PTX and SFN nanocrystals were used as the

controls for the drug release tests. The PTX and SFN powders also served as the controls. For each test, samples of 200 μL were withdrawn at different time points, and the same volume of preheated medium was added back to replace the withdrawn volume. Samples were firstly centrifuged (3 min, 16100g), and then the amount of drug was quantified by HPLC, as described above.

Table S1. The flow rates of inner fluids 1 and 2, and outer fluid with a flow ratio of 1:5:30 in terms of Reynolds numbers.

Reynolds number (Re)	Flow rate (m ³ /s)			
	Inner Fluid 1	Inner Fluid 2	Outer Fluid	Total
10	3.12×10 ⁻¹⁰	1.56×10 ⁻⁹	9.35×10 ⁻⁹	1.12×10 ⁻⁸
50	1.56×10 ⁻⁹	7.79×10 ⁻⁹	4.67×10 ⁻⁸	5.61×10 ⁻⁸
100	3.12×10 ⁻⁹	1.56×10 ⁻⁸	9.35×10 ⁻⁸	1.12×10 ⁻⁷
500	1.56×10 ⁻⁸	7.79×10 ⁻⁸	4.67×10 ⁻⁷	5.61×10 ⁻⁷
1300	4.05×10 ⁻⁸	2.02×10 ⁻⁷	1.21×10 ⁻⁶	1.46×10 ⁻⁶

Table S2. The production rate of SFN@HF with different flow ratios at different Reynolds numbers.

Reynolds number	Total flow rate (m ³ /s)	F1:F2:F3 flow ratio	Production rate (g)	
			SFN (10 mg/mL)	SFN (25 mg/mL)
100	1.12E-07	1:2:6	21.5	53.8
		1:5:30	5.4	13.5
1300	1.46E-06	1:2:6	280.0	700.0
		1:5:30	70.0	175.0

Note: The concentration ratio between SFN and HF is 1:1.

Table S3. DSC characterization of the core/shell nanocomposites prepared by the superfast sequential microfluidic nanoprecipitation platform.

Sample	Dehydration peak/ °C	Melt peak/ °C	Enthalpy $\Delta H/ Jg^{-1}$	Crystallinity/ %
HF	92.7 ± 1.3	–	21.5 ± 0.3	–
PTX	124.9 ± 7.7	–	133.6 ± 3.5	–
PTX-HF PM	122.2 ± 10.8	–	78.2 ± 12.4	~100
PTX@HF	117.2 ± 10.5	–	73.1 ± 1.6	~100
SFN	–	209.9 ± 0.1	96.8 ± 0.3	–
SFN-HF PM	–	202.5 ± 0.1	43.9 ± 0.4	~100
SFN@HF	–	189.3 ± 0.0	43.5 ± 9.5	~100

Note: On PTX@HF DSC profile, no melting endothermic peak has been identified around the PTX melting point, therefore its dehydration endothermic peak was used to calculate the crystallinity of PTX inside the PTX@HF. In the PTX-HF PM, PTX took up of ~44.0% (w/w). Similarly, SFN-HF PM is composed of ~44.5% SFN and ~55.5% of HF.

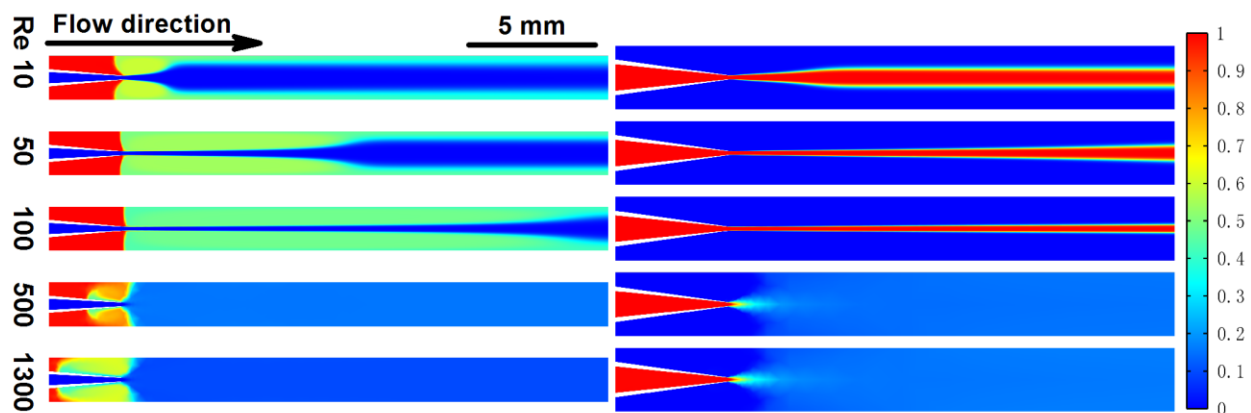


Figure S1. Distribution of normalized concentration. The F1 and F2 are in red and blue for the first mixing process (left side); the mixture of F1 and F2 is in red, and F3 is in blue in the second mixing process (right side). The color bar represents normalized concentration magnitude within the computational domain.

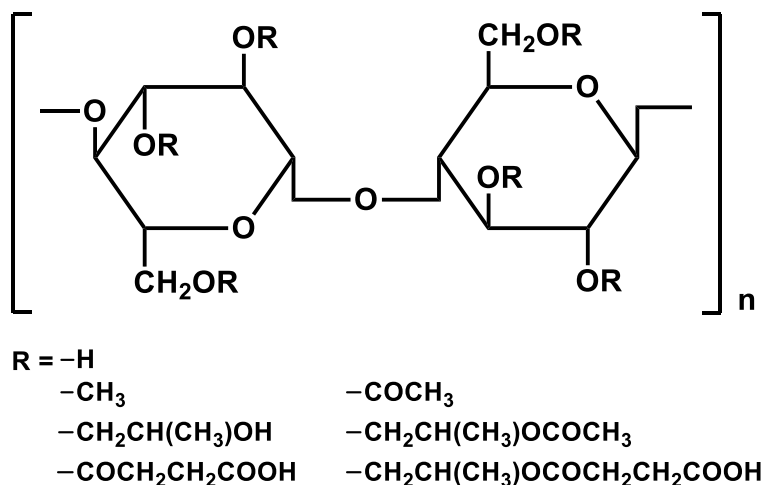


Figure S2. Chemical structure of hypromellose acetate succinate. The pH solubility of different grades is controlled by changing the acetyl and succinoyl group content. The H grade fine powder (HF) dissolves at $pH \geq 6.8$ ⁵.

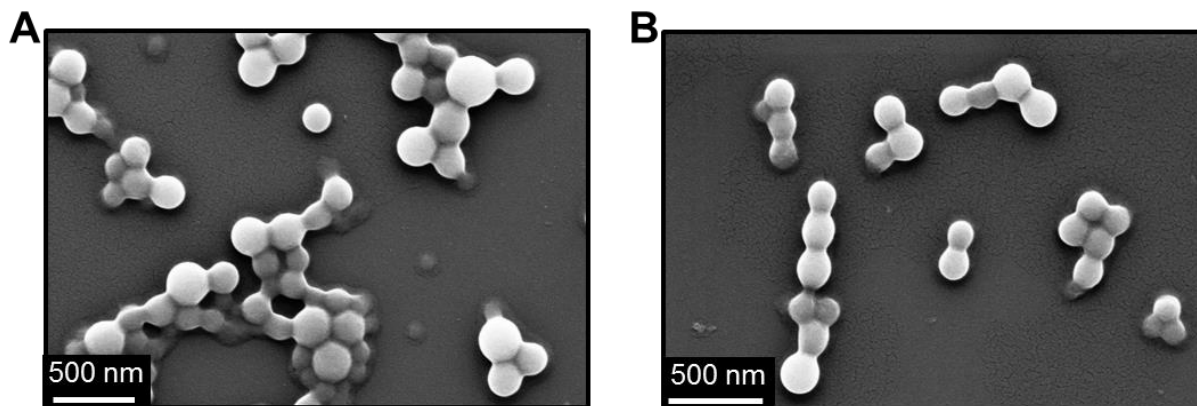


Figure S3. SEM images of nanocomposites. (A) PTX@HF and (B) SFN@HF.

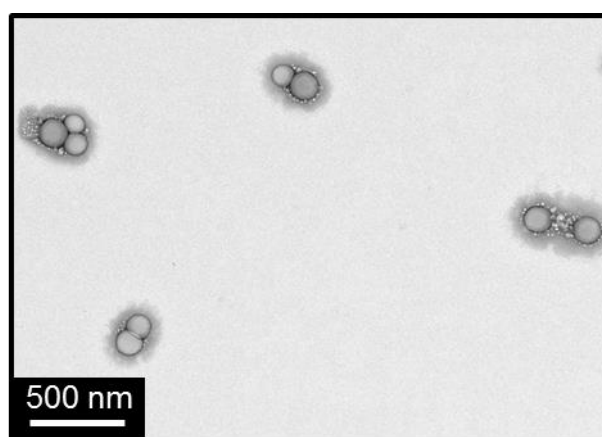


Figure S4. TEM image of PLGA nanoparticles. Nanoparticles prepared by the single step microfluidic nanoprecipitation.

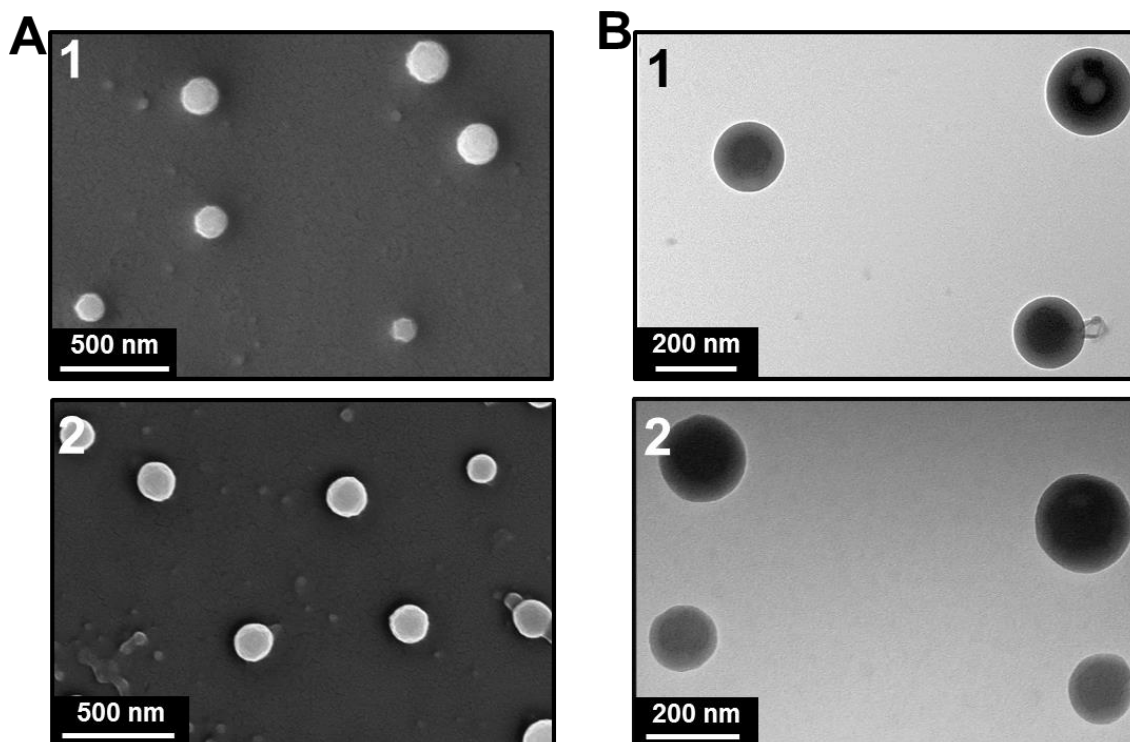


Figure S5. The electron microscopy images of prepared nanocomposites with larger dilution times at Re 100. (A) SEM images of PTX@HF (1) and SFN@HF (2). (B) TEM images of PTX@HF (1) and SFN@HF (2).

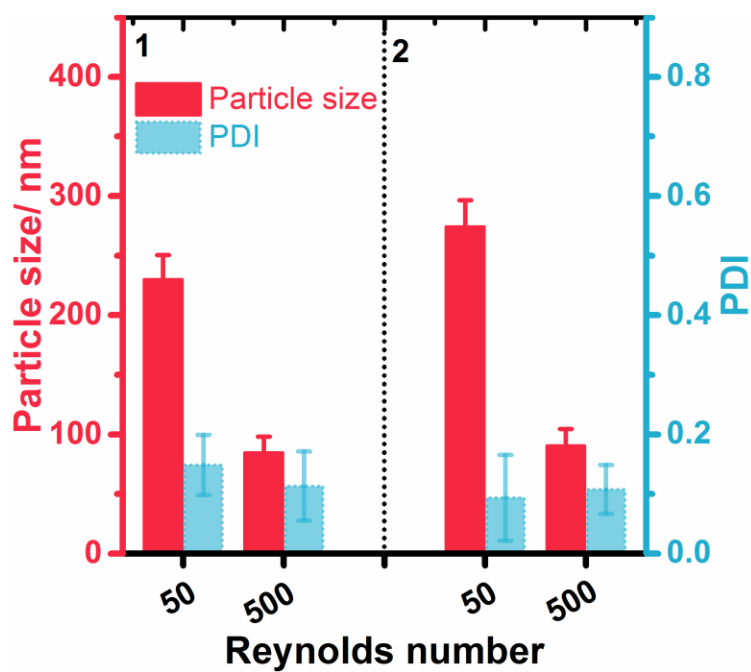


Figure S6. The repeatability of the obtained nanocomposites. The average particle size and size distribution of PTX@HF (1) and SFN@HF (2) at Re 50 and 500 ($n = 22$).

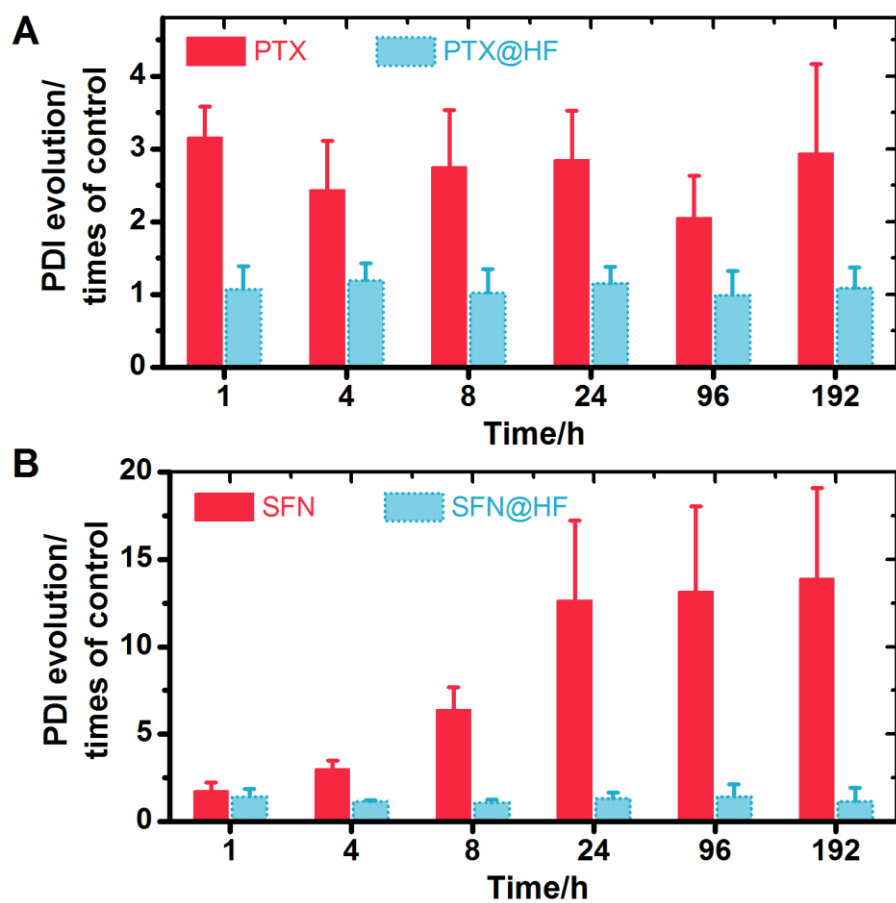


Figure S7. The PDI evolution of prepared nanomaterials over time. (A) PTX nanocrystals and PTX@HF nanocomposites, and (B) SFN nanocrystals and SFN@HF nanocomposites. The average size of the corresponding freshly prepared nanomaterials served as the control ($n = 3$).

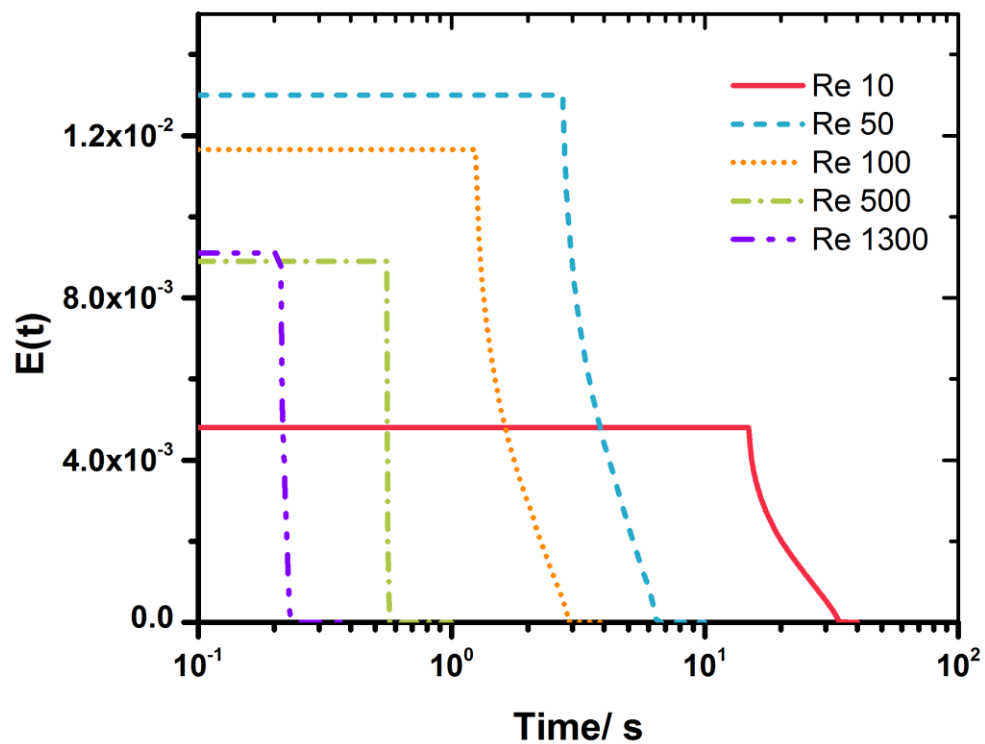


Figure S8. The RTD curve. The residence time distribution of PTX nanocrystals inside the C1.

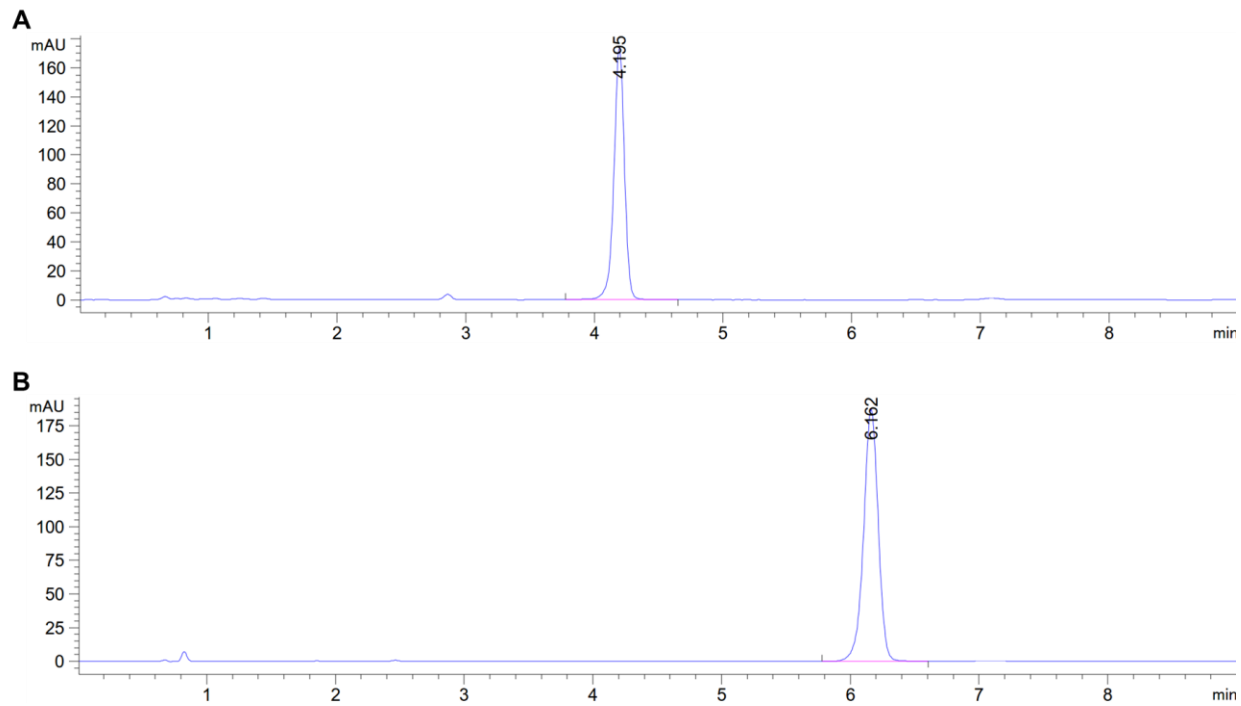


Figure S9. Chromatograms of the loaded therapeutics obtained by reversed phase HPLC.

(A) PTX and **(B)** SFN.

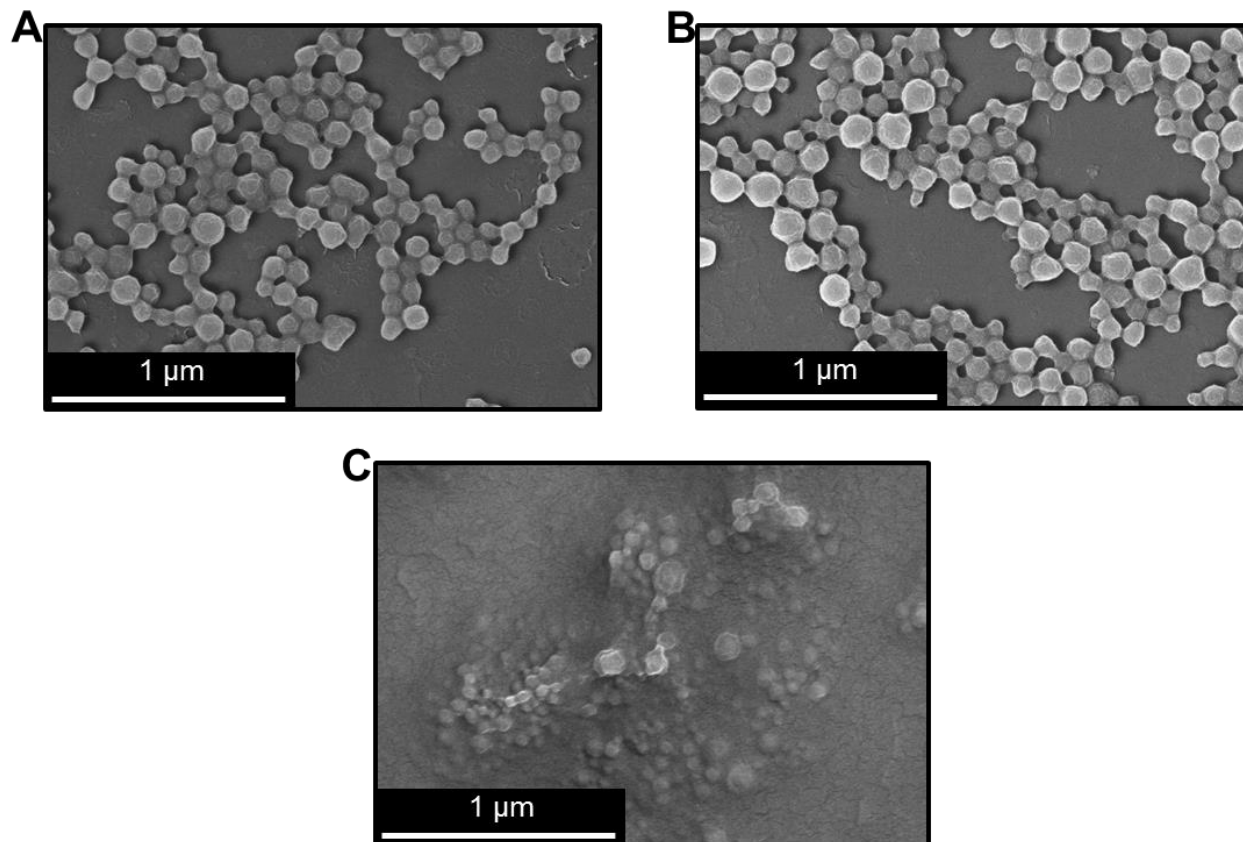


Figure S10. SEM images of bare HF nanoparticles. HF nanoparticles incubated with buffer solutions with a pH value of (A) 1.2, (B) 5.0 and (C) 7.4 for 10 min.

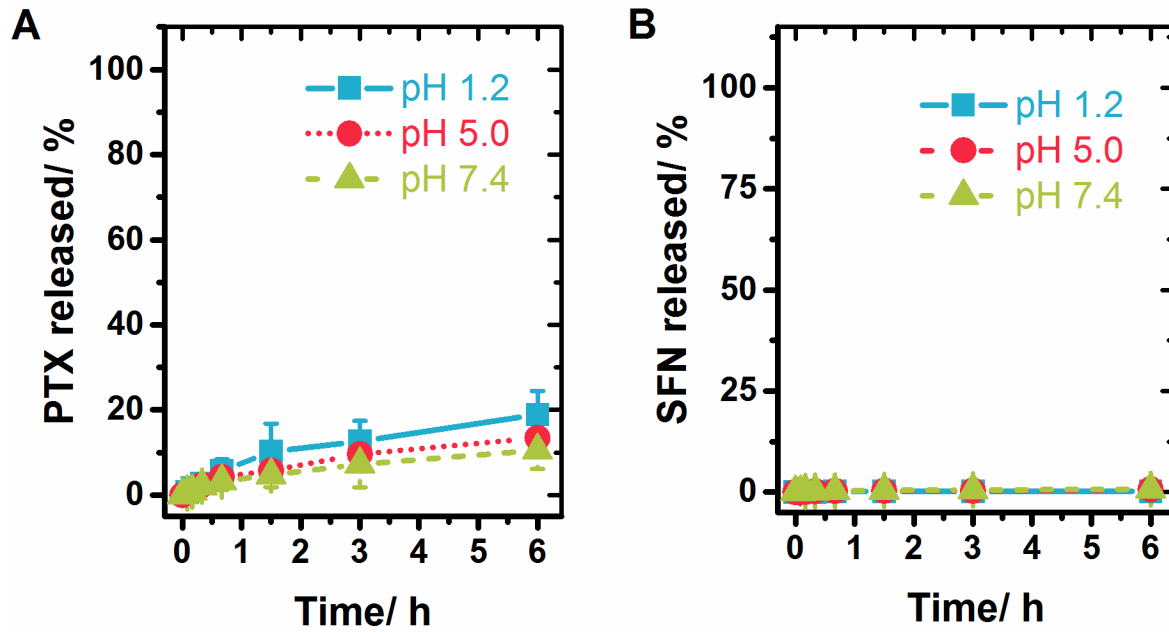


Figure S11. Drug release profiles. The (A) PTX and (B) SFN release profiles from the corresponding bulk powders at pH 1.2, 5.0 and 7.4, respectively ($n = 3$).

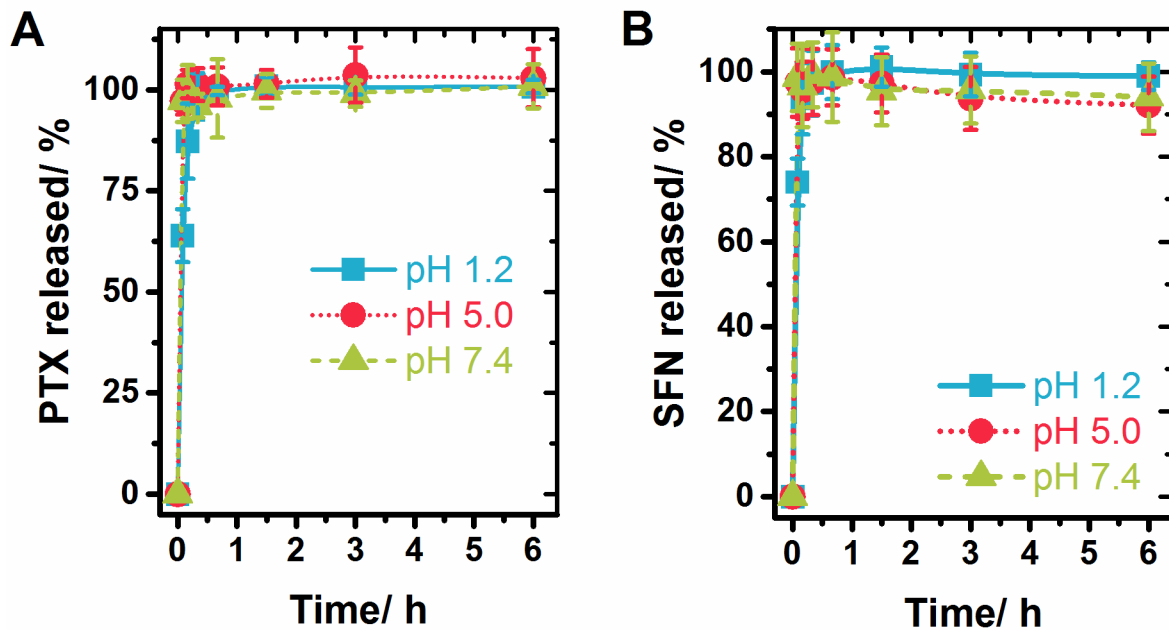


Figure S12. Drug release profiles. The (A) PTX and (B) SFN release profiles from the corresponding freshly prepared drug nanocrystals at pH 1.2, 5.0 and 7.4 ($n = 3$).

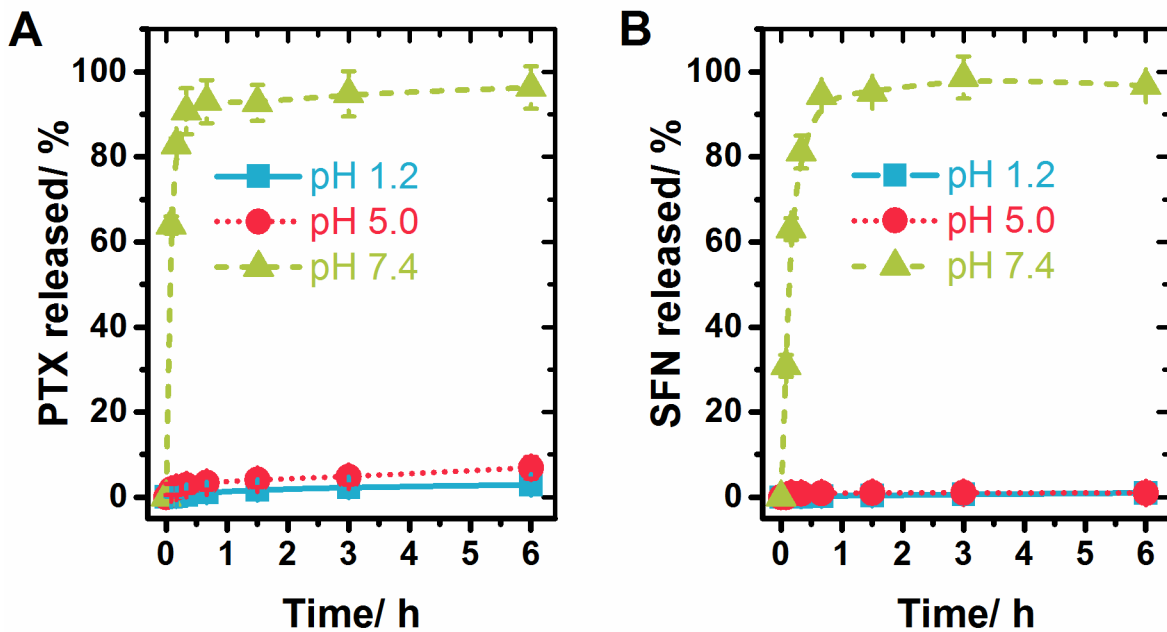


Figure S13. Drug release profiles. The (A) PTX and (B) SFN release profiles from the corresponding core/shell nanocomposites at pH 1.2, 5.0 and 7.4, respectively ($n = 3$).

References

- (1) Kim, Y. T.; Chung, B. L.; Ma, M. M.; Mulder, W. J. M.; Fayad, Z. A.; Farokhzad, O. C.; Langer, R. *Nano Lett.* **2012**, 12, 3587-3591.
- (2) Liu, D. F.; Cito, S.; Zhang, Y. Z.; Wang, C. F.; Sikanen, T. M.; Santos, H. A. *Adv. Mater.* **2015**, 27, 2298-2304.
- (3) Broaders, K. E.; Cohen, J. A.; Beaudette, T. T.; Bachelder, E. M.; Frechet, J. M. J. *Proc. Natl. Acad. Sci. USA* **2009**, 106, 5497-5502.
- (4) Cohen, J. L.; Schubert, S.; Wich, P. R.; Cui, L.; Cohen, J. A.; Mynar, J. L.; Frechet, J. M. J. *Bioconj. Chem.* **2011**, 22, 1056-1065.
- (5) Sarode, A. L.; Obara, S.; Tanno, F. K.; Sandhu, H.; Iyer, R.; Shah, N. *Carbohydr. Polym.* **2014**, 101, 146-53.